

# Variance reduction in coarse bifurcation analysis of stochastic models

Pieter Van Nuffel

April 15, 2016

## Abstract

We investigate the emergence of coarse equilibrium states in a stochastic system of  $p$  system of diffusion processes have a stabilizing force acting on each of them, corresponding to a bistable potential.

We develop a Newton-Krylov method that is able to compute accurately and efficiently coarse fixed points when the underlying fine-scale dynamics is stochastic. The main novelty of the algorithm is in the elimination of the noise that is generated when estimating Jacobian-vector products using time-integration of perturbed initial conditions. We present numerical results that demonstrate

## 1 Problem

As a toy problem we use a model where the closed model is exact. In general, we are interested in performing a bifurcation analysis for a model for which at which an exact, closed model at the macroscopic level is not available.

### 1.1 Model problem

We look for solutions of partial differential equations of advection-diffusion-type

$$\frac{\partial \rho(x, t)}{\partial t} + \mu \frac{\partial (f(x) \rho(x, t))}{\partial x} = \frac{\sigma^2}{2} \frac{\partial^2 \rho(x, t)}{\partial x^2} \quad (1)$$

in two ways:

- By explicitly solving eq. (1) using the discretization scheme<sup>1</sup>

$$\rho_i^{n+1} = \rho_i^n + \Delta t \left( \frac{\sigma^2}{2\Delta x^2} (\rho_{i+1}^n - 2\rho_i^n + \rho_{i-1}^n) - \mu \frac{f(x)}{\Delta x} (\rho_i^n - \rho_{i-1}^n) \right) \quad (2)$$

for the value of the probability density  $\rho$  at position  $x = i\Delta x$  and time  $t = (n+1)\Delta t$ .

---

<sup>1</sup>First-order upwind scheme for the advective part combined with the Forward-Time Central-Space-method for the diffusive part

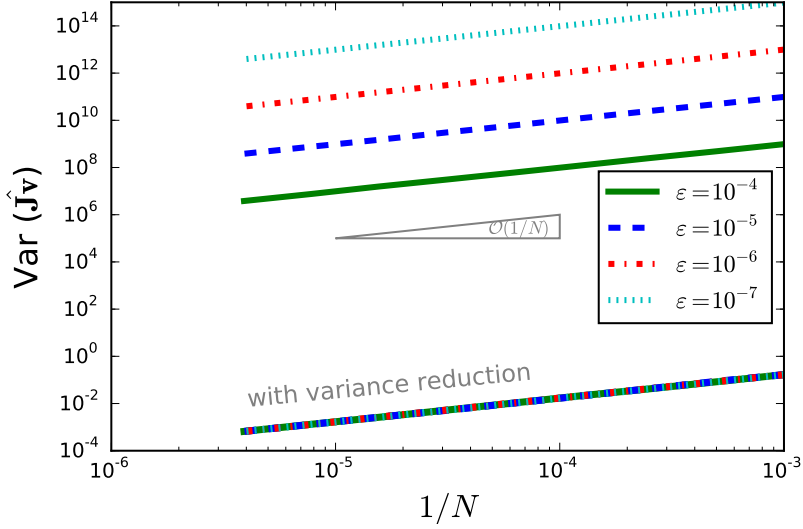


Figure 1: In the case of unweighted restriction, the variance on the stochastic solution of the Jacobian-vector-product becomes unbounded as we decrease the perturbation size  $\epsilon$ . By using weights in the restriction step, the variance does not longer depend on the value of  $\epsilon$  and converges to zero with  $\mathcal{O}(1/N)$ .

- By simulating an ensemble of  $N$  particles evolving according to the corresponding stochastic differential equation

$$dX = \mu f(X)dt + \sigma dW_t. \quad (3)$$

The position  $X^{n+1}$  of each particle at time  $t = (n+1)\Delta t$  is simulated using the Euler-Maruyama scheme

$$X^{n+1} = X^n + \mu f(X^n)\Delta t + \sigma\sqrt{\Delta t} \cdot \xi^n \quad (4)$$

with  $\xi^n \sim \mathcal{N}(0,1)$

## 1.2 Discretization

# 2 Method

## 2.1 Coarse time stepper

To simulate the time evolution of the density  $\rho(t)$ , we construct a coarse time stepper  $\Phi_T^N$  which allows the performance of time-steps at the macroscopic level, using only the stochastic simulation of the position vectors of the  $N$  particles at the microscopic level, generated by eq. (4).

To achieve this, we will define two operators (lifting in subsection 2.1.1 and restriction in subsection 2.1.2) that relate the microscopic and macroscopic levels of description. Once

these lifting  $\mathcal{L}$  and restriction operators  $\mathcal{R}$  have been constructed, a coarse time-stepper  $\Phi_T^N$  to evolve the macroscopic state  $\rho$  over a time interval of length  $n\Delta t$  is constructed as a three-step-procedure (lift-evolve-restrict):

$$\rho(t + n\Delta t) = \Phi_T^N(\rho) = (\mathcal{R} \circ \mathcal{E}(n\Delta t) \circ \mathcal{L}(\omega))(\rho(t)) \quad (5)$$

where  $\mathcal{E}(n\Delta t)(\rho(t))$  is the simulation of the SDE for  $N$  particles over  $n$  timesteps.

### 2.1.1 Lifting: $\rho \rightarrow \mathbf{X}$

Given the density  $\rho$ , we need to sample a position vector  $X_i$  for every particle  $i \leq N$ . We compute  $X$  from a  $N$ -dimensional vector  $\mathbf{U}$  with uniform random elements  $U_i \in [0, 1]$  such that  $\rho(X_i) = U_i$ , using the inverse transformation method. The particle does not only gets an initial position, but also a seed for generating random steps in the simulation.

### 2.1.2 Restriction: $\mathbf{X} \rightarrow \rho$

The restriction operator  $\mathcal{R} : \mathbb{Q}^N \rightarrow \mathbb{Q}^k$  maps the microscopic state  $\mathbf{X}$  (determined by the position vectors of  $N$  particles) to a density  $\rho$ , discretized in  $k$  bins. This is done by counting the number of particles in every bin  $\Delta_j$  for  $1 \leq j \leq k$ :

$$\frac{1}{N} \sum_{i=1}^N w^i \cdot \chi_{\Delta_j}(X^i) = \rho_j \quad (6)$$

with

$$\chi_{\Delta_j}(X) = \begin{cases} 1 & \text{if } X \in \Delta_j, \\ 0 & \text{if } X \notin \Delta_j. \end{cases} \quad (7)$$

and setting all weights  $w_i = 1$  for  $1 \leq i \leq N$ .

The reason why we explicitly introduced these weights in the restriction operator will be clarified in section 11 where we will need to evaluate the coarse time stepper  $\Phi_T^N(\rho + \varepsilon \mathbf{v})$ , now applied to the density shifted with a certain perturbation  $\varepsilon \mathbf{v}$ . To evaluate the perturbed restriction-operator we will use the weights  $w_\varepsilon^i$ , determined such that

$$\frac{1}{N} \sum_{i=1}^N w_\varepsilon^i \cdot \chi_{\Delta_j}(X^i) = \rho_j + \varepsilon v_j. \quad (8)$$

We do this by computing the weight per bin as  $w_\varepsilon^j = 1 + \frac{\varepsilon v_j}{\rho_j}$  and assign this value to each particle in  $\Delta_j$ . So, small perturbations on the density lead to small perturbations in the weights. The advantage of this weighted restriction operator lies in the possibility to use the same realizations  $\mathbf{X}$  in the unperturbed (6) and the perturbed (8) restriction-operator.

## 2.2 Newton-Krylov solver

If we want to compute steady states for the density  $\rho_*$  without direct simulation, we can find them by solving the non-linear system

$$F(\rho_*) = \rho_* - \Phi_T^N(\rho_*) = 0. \quad (9)$$

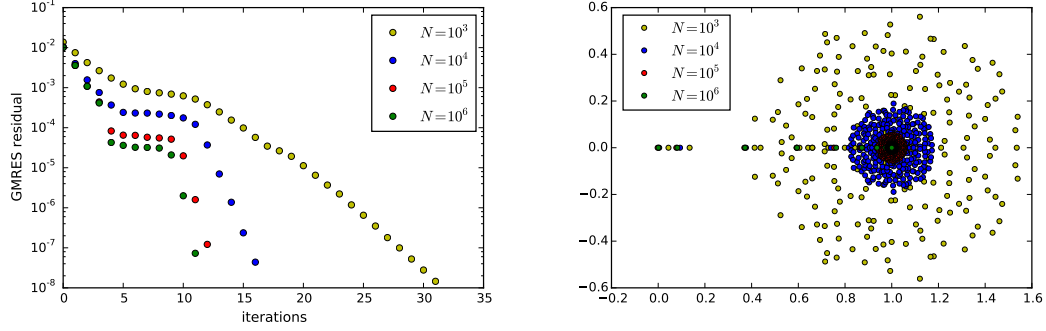


Figure 2: *Left:* The linear iterations necessary to obtain convergence decrease as we increase the number of particles  $N$ . *Right:* The linear iterations necessary to obtain convergence depends on the spectrum of the eigenvalues of the Jacobian. The clustering radius  $\rho$  decreases as we increase the number of particles  $N$ .

To find the steady state  $\rho_*$ , we apply Newton's method to eq. 9. Starting from an initial state  $\rho^0$ , we iterate

$$\begin{cases} \text{Solve } J(\rho^n)\delta_n = -F(\rho^n) \\ \text{Set } \rho^{n+1} = \rho^n + \delta_n \end{cases} \quad (10)$$

until convergence.  $J(\rho^n) = F'(\rho^n)$  denotes the system Jacobian. Each Newton iteration  $n$  thus involves evaluating the Jacobian of the timestepper  $J(\Phi_T^N(\rho))$ . Since we do not have an explicit formula for  $J(\Phi_T^N)$ , we are forced to use an iterative method, such as GMRES, that only requires Jacobian-vector products. [1]. The Jacobian  $J(\Phi_T^N)$  applied to a vector  $\mathbf{v}$  (with unit norm) will be estimated by a finite difference approximation

$$\begin{aligned} J(\Phi_T^N) \cdot \mathbf{v} &\approx \frac{\Phi_T^N(\rho + \varepsilon \mathbf{v}, \omega_1) - \Phi_T^N(\rho, \omega_2)}{\varepsilon} \\ &\approx \frac{\Phi_T^N(\rho, \omega_1) + \varepsilon J(\Phi_T^N)(\rho, \omega_1) \cdot \mathbf{v} - \Phi_T^N(\rho, \omega_2)}{\varepsilon} \end{aligned} \quad (11)$$

### 2.2.1 Analysis of GMRES

The  $k$ th GMRES iteration minimizes the residual  $r = \|x - Ax\|$  over  $x_0 + \mathcal{K}_k$ , where  $x_0$  is the initial iterate and  $\mathcal{K}_k$  is the  $k$ th Krylov subspace  $\mathcal{K}_k = \text{Span}\{r_0, J \cdot r_0, \dots, J^{k-1} \cdot r_0\}$ . Clearly, (fast) matrix-vector products play a crucial role in generating this sequence since each subsequent vector in the sequence is obtained from the previous one by multiplication by  $A$ .

### 2.2.2 experiments

For  $N = 1e6$  particles and  $\Delta_T = 0.1$ : variance and bias becomes lower, for decreasing GMRES-tolerance, until  $\epsilon_{GMRES} = 1e-6$ , then blow-up was observed.

To get a better understanding of the convergence behaviour of the GMRES-method, we refer to the following theorem.

**Theorem 1** (Proof in [2] and [3]). Let  $\mathbf{A} \in \mathbb{C}^{n \times n}$  and assume it has  $m$  distinct eigenvalues  $\lambda_i$  clustered so that for some  $\rho > 0$  and  $z \in \mathcal{C}$ ,  $|\lambda_i - z| \leq \rho$ , together with  $p$  eigenvalues  $\mu_i$  (outliers), each of multiplicity  $m_j$  and each lying outside the cluster  $|\mu_i - z| > \rho$ . Let  $d = \sum_{j=1}^p m_j$  so that  $n = d + m$ . Then, if GMRES is applied to a set of equations with such a matrix of coefficients, it follows, for  $k > 0$ ,

$$\|\mathbf{r}_{d+k+1}\| \leq C \left( \frac{\rho}{|z|} \right)^k \|\mathbf{r}_1\|, \quad (12)$$

where  $C$  is a constant not depending on  $k$ .

The theorem states that GMRES may behave as if it were a two-stage process. In the first phase the terms due to the outliers are eliminated before rapid linear convergence sets in for the second phase. The rate of convergence in this second stage is determined by  $\frac{\rho}{|z|}$ , where  $z$  represents the center of the cluster and  $\rho$  its radius. The closer  $z$  is to the origin, the slower the expected convergence of the algorithm. If the radius of the cluster  $\rho$  is small, we expect a faster convergence of the algorithm. This is observed in figure 2.

### 2.3 Variance reduced Jacobian-vector products

If we use the solution of the PDE, eq. (2), the time stepper is deterministic and the calculation of the Jacobian-vector products is straightforward. If we use the solutions of the SDE however, we have to deal with numerical noise in evaluating eq. 11. Because the coarse time-stepper is stochastic, repeating  $\Phi_T^N$  with two sets of random numbers ( $\omega_1$  and  $\omega_2$ ) will give different results. For  $\varepsilon \ll 1$  this will result in an  $\mathcal{O}(1/(\varepsilon^2 N))$  variance. Consequently the variance on the Jacobian-vector-products will grow unboundedly as  $\varepsilon$  tends to zero and  $J(\Phi_T^N) \cdot \mathbf{v}$  completely loses the structure of the perturbation  $\mathbf{v}$ .

This numerical noise can be reduced by using the same random numbers  $\omega$  for the unperturbed and perturbed simulations. If we apply the weighted restriction operator (8), we get the same microscopic realizations in the lifting step - the only difference is in the computation of the weights. As such, we impose  $\omega_1 = \omega_2$  in eq. (11) and consequently the variance of  $J(\Phi_T^N) \cdot \mathbf{v}$  is bounded and of  $\mathcal{O}(1/N)$ . In the limit of infinitely many particles, the result will converge to the exact Jacobian-vector product. For finite values of  $N$ , there will be noise in the Jacobian-vector product as a result of the random selection of a subset of all possible realizations. The presented procedure only prevents noise blowup that would arise if a different selection of realizations were considered for the perturbed and unperturbed coarse time-step.

## 3 Analysis

### 3.1 Variance

Fig. 3 shows that the variance on the stochastic solution for the Jacobian-vector-product converges to zero with  $\mathcal{O}(1/N)$  and that it does not depend on the value of  $\varepsilon$ .

The convergence of the density to the real solution, strongly depends on the number of particles  $N$  and on the choice of  $\varepsilon$  in the GMRES-method.

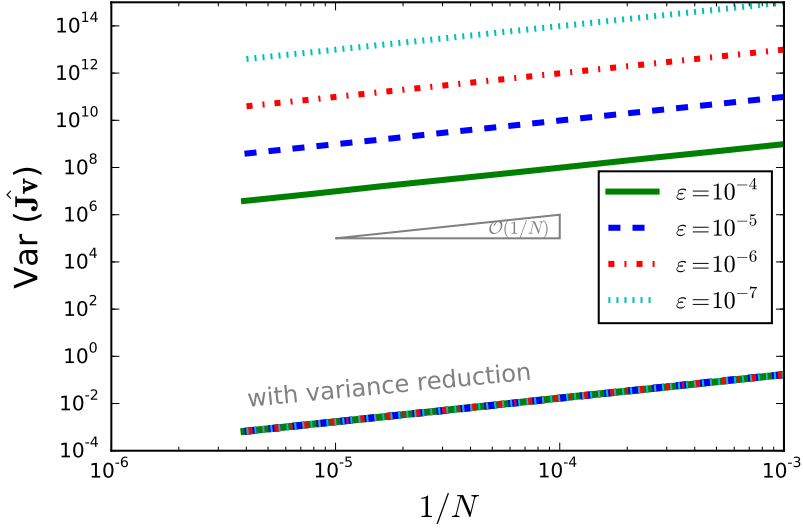


Figure 3: In the case of unweighted restriction, the variance on the stochastic solution of the Jacobian-vector-product becomes unbounded as we decrease the perturbation size  $\epsilon$ . By using weights in the restriction step, the variance does not longer depend on the value of  $\epsilon$  and converges to zero with  $\mathcal{O}(1/N)$ .

### 3.2

### 3.3 bias

## 4 Application: Systemic Risk

Until now, we considered a system of non-interacting particles. We will now extend our model to a mean field model by introducing a third parameter  $\alpha$ , which is the degree of interaction or cooperation in the system. A simple form of cooperative behaviour is the case where each agent tends to follow the state of the majority (or, each particle feels an attractive force towards the mean state of the system). To include this cooperation effect in our stochastic simulation, we add this mean reversion term to the SDE (3):

$$dx = \mu V(x)dt + \sigma dW_t + \alpha(\bar{x} - x)dt, \quad (13)$$

with  $\bar{x}(t) = \frac{1}{N} \sum_{i=1}^N x_i(t)$  denoting the empirical mean.

An interesting application of this model to banks and insurance is the emergence of systemic risk. Banks will try to minimize their own individual risk by spreading the risk between each other. However, this may increase the risk that they may all fail: reducing individual risk on a micro-scale can increase systemic risk on a macro-scale. Garnier, Papanicolaou and Yang already made use of the dynamics in eq. (13) to show that interconnectedness between agents indeed affects the stability of the whole system, causing systemic risk [4]. They defined  $x_i$  as

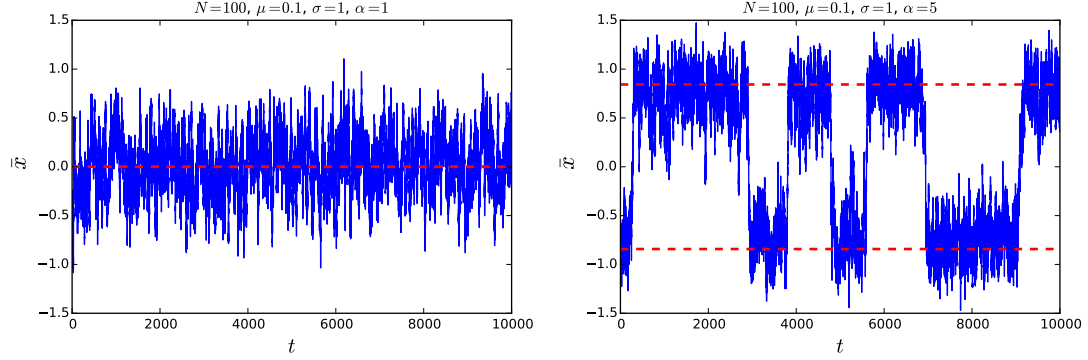


Figure 4: The empirical mean, simulated for different  $\alpha$ . *Left*: the system has one single state  $\bar{x} = 0$ . *Right*: for  $\alpha > \alpha_c$  two metastable equilibria emerge. The red dashed lines are approximated analytical solutions for the steady states.

Table 1: Parameter values

| <i>Discretization parameters</i> |            | SDE       |
|----------------------------------|------------|-----------|
| Discretization step              | $\Delta x$ | $10^{-2}$ |
| Number of discretization steps   | $n_x$      | 340       |
| Time step                        | $\Delta t$ | $10^{-2}$ |
| Number of timesteps              | $n$        | $10^6$    |

the state of risk of agent  $i$ . The bi-stable-state structure of the potential  $V(x)$  ensures that each risk variable stays around  $-1$  (defined as the normal state) or  $+1$  (the failed state). A natural measure of systemic risk is then the transition probability of the empirical mean  $\bar{x}$  from the normal state to the failed state.

To establish the idea, let us repeat the numerical simulations with eq. 13. The evolution of the system is now characterized by the initial conditions, the three parameters  $(\mu, \sigma, \alpha)$  and by the system size  $N$ . Figure 4 illustrates the behavior of the empirical mean  $\bar{x}$ . The simulations were performed with all agents initially in the normal state. Nevertheless, if randomness dominates the interaction, the agents can move immediately to the other potential well. The system then behaves like  $N$  independent diffusions, and hence, by the symmetry of the potential, the mean state will be attracted to a single mixed state  $\bar{x} = 0$ . Upon increasing the interaction parameter  $\alpha$ , however, we find two new macroscopic states, suggesting the presence of a pitchfork bifurcation at the macroscopic level. These solutions are no stable steady states, but rather coarse metastable states. Their lifetime is linked to the finite system size.

## 4.1 Bifurcation study

### 4.1.1 Nota's

Tijdens elke continueringsstap, wordt een nieuw punt gecreëerd dat initieel de dichtheid  $\rho$  krijgt van het vorig punt en met een parameter (D) die horizontaal word geupdate. Dan wordt de norm van het residu berekend  $\|\rho(t) - \rho(t + \Delta t)\|$ , waarin de dichtheid op de volgende tijdsstap verkregen wordt door een simulatie van het systeem met de nieuwe parameter. De grootte van het residu is dus afhankelijk van de stapgrootte in de bifurcatieparameter. De newtontolerantie is de norm van het residu. Als de newton-tolerantie te groot gekozen wordt (in vergelijking met de stapgrootte van het residu), dan wordt er geen Newton-iteratie uitgevoerd. Als de Newton-tolerantie evenwel te klein gekozen wordt, dan bereikt de Newton-solver mogelijk geen convergentie ten gevolge van de ruis. De Newton-tolerantie moet dus weloverwogen gekozen worden.

## 4.2 Results for the pde

Ook hier zien we dat de keuze van de newtontolerantie belangrijk is (te groot = kans op dezelfde toestanden, te klein = failed iterations). Dit kan echter opgevangen worden door de oplossing van dx nauwkeuriger te maken door de tolerantie van de GMRES te verfijnen (het probleem was dat er dx=0 oplossingen werden teruggegeven)

### 4.2.1 Calculating fixed points

The steady states are computed with the Newton-Krylov solver described in section 2.2 and compared with the approximated analytical solutions, calculated by Garnier et. al for small  $h$  [4].

### 4.2.2 Continuation

We use a pseudo-arclength continuation method with secant prediction steps. In fig. ?? we show a bifurcation diagram of the densities.

By adding the mean reversion term, the Fokker-Plack equation (1) describing the evolution of the density, now becomes

$$\frac{\partial \rho(x, t)}{\partial t} = -\mu \frac{\partial (V(x) \rho(x, t))}{\partial x} - \alpha \frac{\partial}{\partial x} \left[ \left( \int x \rho(x, t) dx - x \right) \rho(x, t) \right] + \frac{\sigma^2}{2} \frac{\partial^2 \rho(x, t)}{\partial x^2}. \quad (14)$$

Explicit solutions of eq. are not available in general, but we can find equilibrium solutions. Assuming



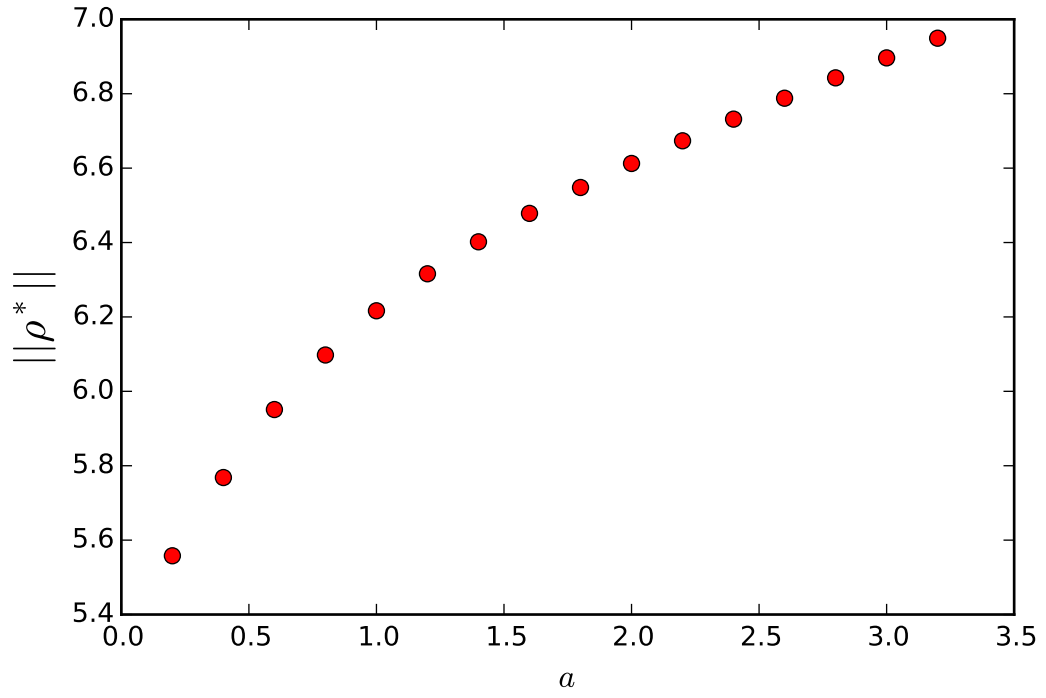


Figure 5: Bifurcation diagram of the steady states calculated with the Newton-Krylov-Solver for the PDE.  $\Delta t = 10^{-4}$ ,  $\Delta T = 10^{-2}$ ,  $\Delta x = 10^{-2}$ ,  $\Delta D = 0.01$ ,  $\epsilon_{GMRES} = 10^{-5}$ ,  $\delta_{Newton} = 10^{-7}$ ,  $\epsilon = 10^{-5}$

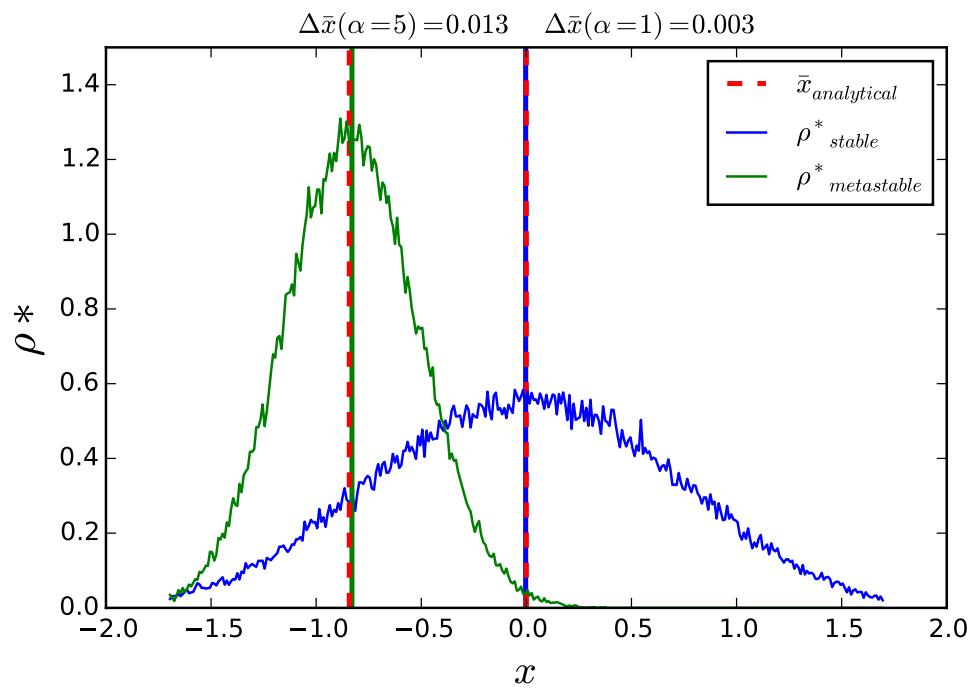


Figure 6

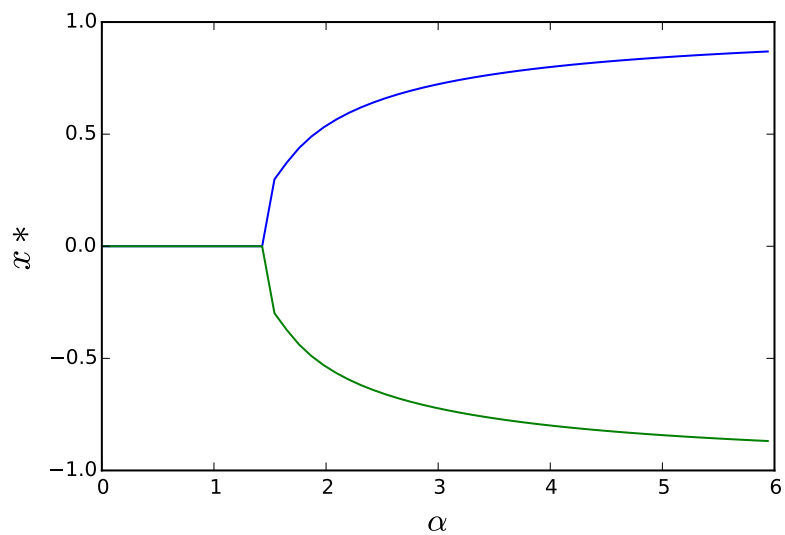


Figure 7

## 5 Newton convergence

### References

- [1] Peter N. Brown and Youcef Saad. Hybrid krylov methods for nonlinear systems of equations. *SIAM J. Sci. Stat. Comput.*, 11(3):450–481, May 1990.
- [2] C.G. Broyden and M.T. Vespucci. *Krylov Solvers for Linear Algebraic Systems: Krylov Solvers*. Studies in Computational Mathematics. Elsevier Science, 2004.
- [3] S. L. Campbell, I. C. F. Ipsen, C. T. Kelley, and C. D. Meyer. GMRES and the minimal polynomial. *BIT Numerical Mathematics*, 36(4):664–675, dec 1996.
- [4] Josselin Garnier, George Papanicolaou, and Tzu-Wei Yang. Large deviations for a mean field model of systemic risk. Papers 1204.3536, arXiv.org, April 2012.